

Topology optimization considering static failure theories for ductile and brittle materials[☆]

Seung Hyun Jeong^a, Seon Ho Park^a, Dong-Hoon Choi^b, Gil Ho Yoon^{b,*}

^a Graduate School of Mechanical Engineering, Hanyang University, Republic of Korea

^b School of Mechanical Engineering, Hanyang University, Seoul, Republic of Korea

ARTICLE INFO

Article history:

Received 24 November 2011

Accepted 20 July 2012

Available online 15 August 2012

Keywords:

Stress-based topology optimization

Static failure criteria

Brittle material

Ductile material

ABSTRACT

This research develops a stress-based topology optimization method (STOM) that considers various static failure criteria, including those from the maximum shear stress theory, the distortion energy theory, the ductile Coulomb–Mohr theory, the brittle Coulomb–Mohr theory, and the modified Mohr theory for ductile and brittle materials. Due to some theoretical and numerical challenges, the above static failure theories have not been implemented in topology optimization. By substituting failure formulas that are non-differentiable with respect to the stress components and design variables with differentiable approximation formulas, it is possible to utilize these failure criteria to design mechanical structures that minimize mass.

© 2012 Elsevier Ltd. All rights reserved.

1. Introduction

This paper develops a reliable stress-based topology optimization method (STOM) that incorporates the static failure criteria for the brittle and ductile materials denoted in Fig. 1(a). Since the introduction of topology optimization (TO) for continuum stiff structures in the late 1980s, numerous works have investigated its theoretical and practical applications. For example, compared to size and shape optimization methods, optimal topological layouts do not necessarily require the initial designs for various mechanical conditions. Thus, several topology optimization methods, such as the homogenization based method [1–6], the solid isotropic with penalization (SIMP) method [7–9], the level set method [10–15], and the element connectivity parameterization (ECP) method [16–21], have been developed and applied to a variety of engineering problems. Unfortunately, few studies give enough investigation into the topology optimization of element-wise stress constraints as well as the various static and dynamic failure criteria, which are mathematically not differentiable with respect to both the TO design variables and the principal stresses. Consequently, this paper presents a new TO framework that utilizes the STOM for the static failures given in Fig. 1 by introducing differentiable formulations of these static criteria with differentiable maximum and minimum operators (as shown in Fig. 1(b)). The design variable in Fig. 1 is density assigned to each element in design

domain to determine whether an element in design domain should be modeled as void or solid. The number of the design variables is NE . If the design variable γ_e approaches to its lower bound, the e th element should be modeled as “void”. Otherwise, if the design variable approaches to one, the e th element should be modeled as “solid.” Also, $g_e^{(\odot)}$ in Fig. 1 represents the failure criterion of ductile or brittle material and explained in detail in the section 2.

It is still difficult to consider both the static failure and the dynamic failure (i.e. fatigue) in TO. Among the several static failure criteria listed in Fig. 1, the distortion energy (DE) theory – also called the von Mises stress theory – has been successfully implemented in TO, but only after addressing several significant challenges, including the stress-singularity issue, the many-constraint issue, which makes the use of a gradient-based optimizer difficult, and the highly nonlinear behavior of stress with respect to TO design variables. (See [1,22–31] for more details.) The stress-singularity issue often occurs for two- or three-dimensional finite elements with TO design variables closer to the lower bound. In other words, some finite elements have a weak Young's moduli and thus, may experience excessive distortion. This effect produces a high stress value, which is difficult to optimize topologically. To overcome this difficulty, the ε -relaxation function [25,26], the smooth envelope functions (SEFs) [32], and the relaxed stress indicator [27] have been proposed. Recently, in [33–37], the different tension and compression stress limits have been considered for topology optimization. Another challenge of TO is that defining a large number of failure criteria for every element is a sub-optimization problem, which is difficult for a gradient-based optimizer to solve efficiently. To resolve this challenge, a p -norm approximation, which aggregates many constraints into one global constraint, has been

[☆] This work was supported by the National Research Foundation of Korea (NRF) grant funded by the Ministry of Education, Science and Technology (No. 2012-0005530) and (No. 2011-0027359).

* Corresponding author.

E-mail addresses: ghy@hanyang.ac.kr, gilho.yoon@gmail.com (G.H. Yoon).

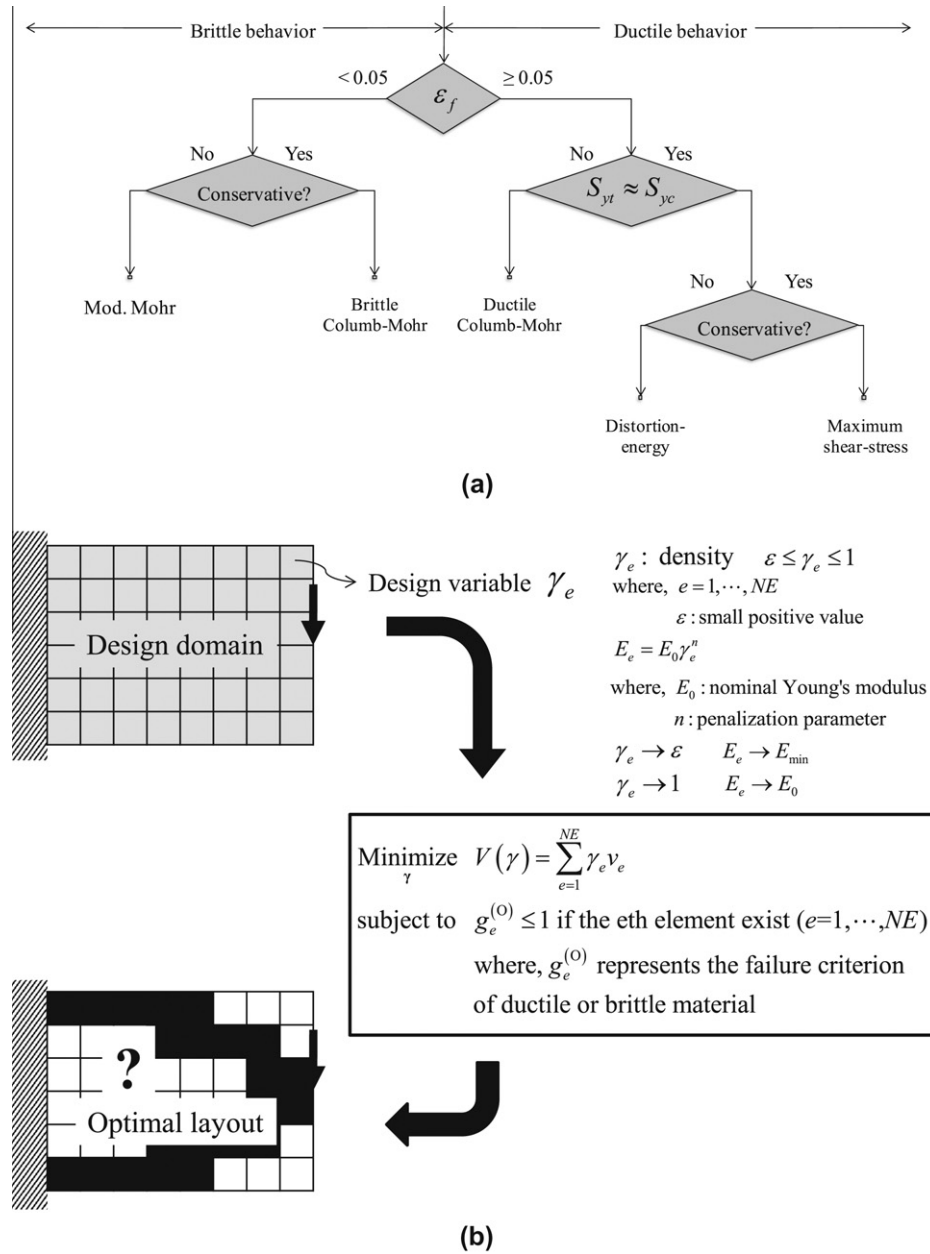


Fig. 1. (a) The diagram of static failure criteria for ductile and brittle materials and (b) the topology optimization minimizing the usage of volume, subject to static failure constraints for ductile or brittle materials (the design variables defined at every finite element are denoted by γ).

proposed. However, since there are disadvantages to a global constraint function, several researchers [27–29,38] have proposed calculating the global constraints as segregated subdomains. Finally, the issue of the highly non-linear behavior of the stress constraint has been studied extensively in [39]. According to this research, a highly non-linear stress constraint is often observed when relaxation techniques are employed to cope with the singularity issue. Consequently, the aforementioned challenges clearly highlight the complexity of obtaining global optima through stress-based topology optimization. Yet, after addressing some of these challenges, this paper discusses the recent advances making it possible to conduct TO with DE failure theory.

Additional phenomenological failure criteria between strength (a property or characteristic of a mechanical element) and static load (a stationary or coupled force applied to a member) for brittle and ductile materials are shown in Fig. 1. Since no previous TO research considers these phenomenological failure criteria, it

becomes important to consider the other static failure criteria in TO as well – i.e., the maximum shear stress (MSS) theory, the ductile Coulomb–Mohr (DCM) theory, the brittle Coulomb–Mohr (BCM) theory, and the modified Mohr (MM) theory, as listed in Figs. 1 and 2. Hence, this paper develops a new topology optimization framework utilizing the differentiable failure criteria with respect to the TO design variables. Note, however, that there are some non-differentiable points for these criteria, as shown in Fig. 2.

One of difficult features when considering these failure criteria in TO (except the von Mises stress criterion) is that the mathematical formulations of these static failure criteria have a maximum operator, a minimum operator, and a logical if operator, which are all non-differentiable with respect to both the TO design variables and the principal stress values, as shown in Fig. 2. For example, the MSS theory for the plane stress element is non-differentiable with respect to the principal stress values when the principal stresses, σ_A and σ_B (unsorted principal stresses), become (S_y, S_y) , $(0, S_y)$, $(0, -S_y)$, $(S_y, 0)$,

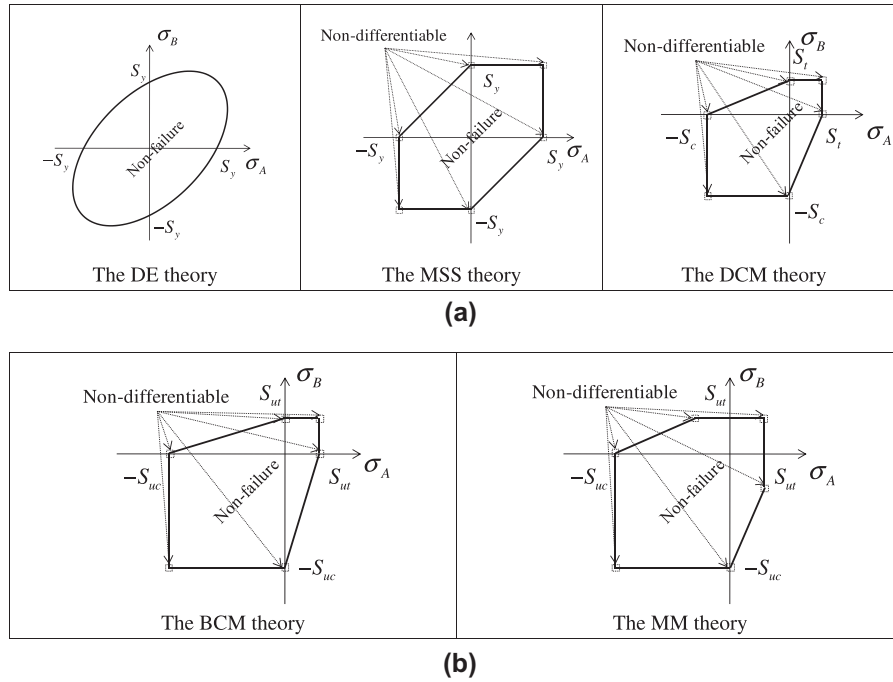


Fig. 2. Graphs of the failure envelopes of plane-stress elements for ductile and brittle materials: (a) The failure envelopes using the MSS theory, the DE theory and the DCM theory for ductile material and (b) the failure envelopes using the BCM theory and the MM theory for brittle material. (The principal stresses: σ_A and σ_B , yield stress: S_y , the compressive strength: S_c , the tensile strength: S_t , the ultimate compressive strength: S_{uc} , the ultimate tensile strength: S_{ut}).

$(-S_y, 0)$, and $(-S_y, -S_y)$. Other criteria also have non-differentiable kinks in their graphs. Furthermore, calculation of the principal stresses requires the maximum and minimum logical operators, which are non-differentiable with respect to the design variables. Since a gradient-based optimizer requires sensitivity values of the objective function as well as stress constraints, it is impossible to conduct TO with the failure criteria without resolving these numerical issues. Hence, by introducing new, differentiable maximum and minimum logical operators, this research reformulates the differentiable static failure criteria for TO.

The layout of this paper is organized as follows: first, the reformulations of the failure theories for TO are introduced and their essential features are explained. Then, in the numerical example section, the significance of considering these failure criteria in TO is demonstrated by solving several topology optimization examples with the developed TO framework. Finally, our findings and some topics for future research are summarized and discussed in the conclusion.

2. Stress-based topology optimization for various material failure criteria

2.1. Topology optimization formulation with static failure criteria

The original topology optimization problem that involves the stress constraint for each element and strives to minimize the material usage is subject to the static failure criterion constraints as follows:

$$\begin{aligned} & \text{Minimize } V\gamma \\ & \text{subject to } g_e^{(\circ)}(\sigma_1, \sigma_2, \sigma_3) \leq 1 \quad \text{if the } e\text{th element exists} \\ & (e = 1, 2, \dots, NE) : \text{Local constraints} \\ & \gamma = [\gamma_1 \cdots \gamma_{NE}] (\varepsilon \leq \gamma_i \leq 1, \varepsilon : \text{a lower bound}) \end{aligned} \quad (1)$$

where the right superscript, \circ , in $g_e^{(\circ)}$ represents DE, MSS, DCM, BCM, or MM depending on the failure criterion of interest, and

where γ denotes the design variables for each element. Originally this topology optimization problem is a binary optimization problem which is one of the hardest engineering optimization problems. Therefore, in order to solve this binary optimization problem within a reasonable computation time, it is common to relax it by adopting the continuum design variables [7,8,40]. The number of design variables or finite elements is denoted by NE . The constraint function associated with each failure theory is given by $g_e^{(\circ)}$, which can be formulated using the principal stresses, σ_1 , σ_2 , and σ_3 .

To evaluate the displacements and the stresses, the general finite element (FE) procedure is adopted as follows:

$$\mathbf{KU} = \mathbf{F} \quad (2)$$

where the global stiffness matrix, the displacement vectors, and the external force are denoted by \mathbf{K} , \mathbf{U} , and \mathbf{F} , respectively. The global stiffness matrix is assembled as follows:

$$\mathbf{K} = \sum_{e=1}^{NE} \mathbf{A} \mathbf{k}_e \quad \text{and} \quad \mathbf{k}_e = \int_{v_e} \mathbf{B}^T \mathbf{C}_e \mathbf{B} dv \quad (v_e : \text{the } e \text{ th element domain}) \quad (3)$$

where the symbol \mathbf{A} represents the assembly FE operator for the element stiffness matrices \mathbf{k}_e . The strain-displacement matrix is denoted by \mathbf{B} . For the plane stress element using solid isotropic material with penalization (SIMP), the constitutive matrix, \mathbf{C}_e , is expressed as follows:

$$\mathbf{C}_e = \frac{E(\gamma_e)}{1-\nu^2} \begin{bmatrix} 1 & \nu & 0 \\ \nu & 1 & 0 \\ 0 & 0 & (1-\nu)/2 \end{bmatrix} \quad (4)$$

$$E(\gamma_e) = E_0 \gamma_e^n \quad (5)$$

where the penalization factor and the nominal Young's modulus are denoted by n and E_0 , respectively. The design variable of the e th element is γ_e . For the two-dimensional plane stress problem, the element-wise stress evaluation is calculated as follows:

$$\sigma_e = {}_s\mathbf{C}_e \mathbf{B}_e \mathbf{u}_e = \{\sigma_{xx}, \sigma_{yy}, \tau_{xy}\} \quad (6)$$

$${}_s\mathbf{C}_e = \frac{E_0 \gamma_e^{n_s}}{1 - \nu^2} \begin{bmatrix} 1 & \nu & 0 \\ \nu & 1 & 0 \\ 0 & 0 & (1 - \nu)/2 \end{bmatrix} \quad (7)$$

$$\sigma^3 - (\sigma_{xx} + \sigma_{yy})\sigma^2 + (\sigma_{xx}\sigma_{yy} - \tau_{xy}^2)\sigma = 0 \quad (8)$$

where the displacements and the constitutive matrix for stress evaluation are denoted by \mathbf{u}_e and ${}_s\mathbf{C}_e$ respectively. Here, the index e of the stress components in (6) is intentionally omitted for simplicity. Note that a different penalty factor, n_s , is used instead of n . The non-zero principal stresses, σ_A and σ_B , for the plane stress elements are the non-zero roots of (8). The previous research [27] suggests using the values of 3 for the penalization factor (n) of the interpolation of the material property and 0.5 for the penalization factor of the stress evaluation (n_s) in order to avoid the singularity issue in this stress-based topology optimization problem. The effects of these two parameters are investigated in the numerical example section.

To address the excessive number of local constraints and the nonlinear characteristics of the stress constraints, the original topology optimization problem (1) can be reformulated by introducing the density filter, the regional (aggregation) scheme of the element-wise constraints, the p -norm formulation, and the other components developed in [27]. The procedure can then be written as follows:

$$\begin{aligned} &\text{Minimize}_{\gamma} V(\tilde{\gamma}) = \sum_{e=1}^{NE} \tilde{\gamma}_e \nu_e(\tilde{\gamma} : \text{Filtered density}) \\ &\text{subject to } \langle g_{\max} \rangle_1 \leq 1 \\ &\quad \langle g_{\max} \rangle_2 \leq 1 \\ &\quad \vdots \\ &\quad \langle g_{\max} \rangle_{RN} \leq 1 \\ &\quad \tilde{\gamma} = \Xi(\gamma) \text{ with the density filter } \Xi \end{aligned} \quad (9)$$

$$\langle g_{\max} \rangle_k = \max (g_e^{(\odot)}) \quad \text{when } e \in \Omega_k \text{ and the } e\text{th element exists} \quad (10)$$

$\odot = \text{DE, MSS, DCM, BCM, or MM}$ depending on a failure criterion of interest

where the maximum value of stress constraints in the k th region is denoted by $\langle g_{\max} \rangle_k$ and the number of subdivided regions for the stress constraint evaluation is RN . In (9), due to the non-differentiable maximum operator, the analytical sensitivity values for a gradient-based approach for topology optimization cannot be driven. To resolve this sensitivity issue, the maximum operator is replaced by the p -norm approximation multiplied by a correction factor at the $iter$ th optimization iteration as follows from [27]:

$$\langle g_{\max} \rangle_k \equiv c_k^{iter} \left(\sum_e (g_e^{(\odot)})^p \tilde{\gamma}_e \right)^{1/p} \quad (e \in \Omega_k) \quad (11)$$

$$\langle g_{PN} \rangle_k \equiv \left(\sum_e (g_e^{(\odot)})^p \tilde{\gamma}_e \right)^{1/p} \quad (e \in \Omega_k) \quad (12)$$

$$c_k^{iter} = \alpha \frac{g_{\max,k}^{iter-1}}{\langle g_{PN} \rangle_k^{iter-1}} + (1 - \alpha) c_k^{iter-1} \quad 0 < \alpha < 1 \quad (13)$$

where c_k^{iter} , $g_{\max,k}^{iter}$ and α are the correction factor at the $iter$ th optimization iteration, the real maximum value of the constraint functions in the k th region, and the damping factor, respectively. Mathematically, non-differentiable operations must be added between the optimization iterations to account for the correction factor and the

density filter. Moreover, the p value used for p -norm approximation should theoretically be infinite to represent the maximum function. However, with a p value that is very large, Eq. (12) produces non-linear characteristics. For this reason, a value between 3 to 4 is recommended for the p value [27]. In fact, numerical examples indicate that the p -norm of the stress constraints likely dictates not only the behavior or the sensitivity information of the maximum stress constraints but also the overall behavior of the stress constraints in a design domain. The parameter α is the numerical damping factor for the stress constraints. Because the aggregated constraints in (11) experiences some oscillations for some iterations, this damping factor is introduced in [27]. With oscillations with a large magnitude, a small value is used for this damping factor. In this research, the value of α is set to 0.5 if not mentioned. Also, the effects of damping factor are investigated in the numerical section.

2.2. Formulations of static failure criteria with phenomenological failure theories

In this subsection, a short explanation and associated formulations of the static failure theories are presented. A thorough description of these failure theories can be found in [41]. According to the phenomenological failure theories established by experimental data from [41], the characteristics of engineering materials can be classified as ductile and brittle depending on the true strain value ε_f at fracture, as shown in Fig. 1. The materials with an ε_f larger than 0.05 are regarded as ductile materials, while the materials with 0 an ε_f smaller than 0.05 are regarded as brittle materials. In the case of brittle materials, there are the two failure theories: the MM theory and the BCM theory. The BCM theory is more conservative than the MM theory, but the failure envelope of the MM theory is larger than that of the BCM theory. In case of ductile materials, there are the three failure theories: the DE theory, the MSS theory, and the DCM theory. The DE and the MSS theories are generally applied for ductile materials whose tension and compression yield strengths are similar to each other, whereas the DCM theory is used to predict failures of materials with different tension and compression yield strengths. Mathematically, the MMS theory is known to be more conservative than the DE theory.

2.2.1. The distortion energy (DE) theory for ductile materials

The DE theory assumes that any structural element has a distortion strain energy per unit volume that exceeds the strain energy of a yielded unit volume in simple tension or compression tests, which can be found using Eq. (14). The DE theory originated from the observations that the yield stress values of ductile materials that had been pressurized hydrostatically were greater than the yield stress values from simple tension or compression tests. A graphical description of the DE theory is given in Fig. 2. As mentioned in the previous sections, all the research for stress-based TO is based on the DE theory because the mathematical formulation of the DE theory is differentiable with respect to both the design variables as well as the principal stress components, which can be shown as

$$\begin{aligned} \sigma &= \left[\frac{(\sigma_1 - \sigma_2)^2 + (\sigma_2 - \sigma_3)^2 + (\sigma_3 - \sigma_1)^2}{2} \right]^{1/2} \\ &= \frac{1}{\sqrt{2}} \left[(\sigma_x - \sigma_y)^2 - (\sigma_y - \sigma_z)^2 - (\sigma_z - \sigma_x)^2 + 6(\tau_{xy}^2 + \tau_{yz}^2 + \tau_{zx}^2) \right]^{1/2} \leq S_y \end{aligned} \quad (14)$$

For the purpose of topology optimization, the $g_e^{(\odot)}$ in (1) can be expressed using the above criterion (Eq. (14)) as in (15):

$$g_e^{DE} = \frac{\frac{1}{\sqrt{2}} \left[(\sigma_x - \sigma_y)^2 - (\sigma_y - \sigma_z)^2 - (\sigma_z - \sigma_x)^2 + 6(\tau_{xy}^2 + \tau_{yz}^2 + \tau_{zx}^2) \right]^{1/2}}{S_y} \leq 1 \quad (15)$$

Note that the upper superscript *DE* is used to indicate that the constraint function in g_e^{DE} in (1) has been formulated with the DE theory.

2.2.2. The maximum shear stress (MSS) theory for ductile materials

Observation of the fracture behaviors in tensile test specimens resulted in the MSS theory. Since fracture lines usually occur approximately 45 degrees from the axis of tensile test specimens (where the shear stress is maximized), the MSS theory assumes that yield phenomena occur when the maximum shear stress in any structural element is equal to or larger than the yield strength. For any structural element having a stress state in the outside domain marked by the dotted line in Fig. 2, it is assumed that the corresponding structural element has been subjected to the static failure as described in the MSS theory. The MSS formulation is based on the maximum and minimum values of the three principal stresses (see Eq. (16)), and consequently, its criterion is non-differentiable with respect to both the design variables of TO as well as the principal stress components.

$$\tau_{\max} = \frac{\max(\sigma_1, \sigma_2, \sigma_3) - \min(\sigma_1, \sigma_2, \sigma_3)}{2} = \frac{\sigma_1 - \sigma_3}{2} \leq \frac{S_y}{2} \quad (16)$$

The maximum and minimum values of the principal stress values are denoted by $\max(\sigma_1, \sigma_2, \sigma_3)$ and $\min(\sigma_1, \sigma_2, \sigma_3)$, respectively. Moreover, it is worthwhile to note that in a real computation, the order of magnitude of the principal stress values should be computed with these non-differentiable logical operators. To formulate TO with the MSS theory, the constraint functions defined for all finite elements should be calculated as follows:

$$g_e^{MSS} = \frac{\max(\sigma_1, \sigma_2, \sigma_3) - \min(\sigma_1, \sigma_2, \sigma_3)}{S_y} \leq 1 \quad (17)$$

2.2.3. The ductile Coulomb–Mohr (DCM) theory for ductile materials

The DCM theory is another failure criterion for ductile material having different tensile and compression yield strengths and sharing many similarities with the MSS theory. For example, in order to determine whether magnesium alloy, whose yield strength in compression (S_c) is less than its yield strength in tension (S_t), has statically failed under a given loading condition, the DCM theory in (18) and Fig. 2 can be used. A detailed derivation and explanation of the DCM theory can be found in [41]. Note that the failure criterion has many similarities to the MSS theory except that different values for compressive and tensile yield strengths are employed.

$$g_e^{DCM} = \frac{\max(\sigma_1, \sigma_2, \sigma_3)}{S_t} - \frac{\min(\sigma_1, \sigma_2, \sigma_3)}{S_c} = \frac{\sigma_1}{S_t} - \frac{\sigma_3}{S_c} \leq 1 \quad (18)$$

Once again, the above equations are not differentiable due to the maximum and minimum operators.

2.2.4. The brittle Coulomb–Mohr (BCM) theory for brittle materials

As explained before, brittle material is subjected to fail with a smaller equivalent strain than ductile material and commonly the two static failure criteria – i.e., those from the BCM and the MM theories – are used to determine the potential failure of a structural element. The BCM theory in Fig. 2(b) also has many similarities with the above DCM theory except that it uses the ultimate strength instead of the yield strength (see Eq. (19)) to calculate plane stress. Thus, it is just a matter of changing the material property.

$$g_e^{BCM} = \frac{\max(\sigma_1, \sigma_2, \sigma_3)}{S_{ut}} - \frac{\min(\sigma_1, \sigma_2, \sigma_3)}{S_{uc}} \leq 1 \quad (19)$$

2.2.5. The modified Mohr (MM) theory for brittle materials

The modified Mohr (MM) theory expands the failure region of the BCM theory in the second and forth quadrants to the envelopes

defined by the lines shown in Fig. 2(b). The mathematical formulations of the MM failure criterion for the plane stress element are defined as follows:

$$\sigma_1 \leq S_{ut} \quad \sigma_1 \geq \sigma_2 \geq 0 \quad (20)$$

$$\sigma_1 \leq S_{ut} \quad \sigma_1 \geq 0 \geq \sigma_2 \quad \text{and} \quad \left| \frac{\sigma_2}{\sigma_1} \right| \leq 1 \quad (21)$$

$$\frac{(S_{uc} - S_{ut})\sigma_1}{S_{uc}S_{ut}} - \frac{\sigma_2}{S_{uc}} \leq 1 \quad \sigma_1 \geq 0 \geq \sigma_2 \quad \text{and} \quad \left| \frac{\sigma_2}{\sigma_1} \right| > 1 \quad (22)$$

$$\sigma_2 \leq -S_{uc} \quad 0 \geq \sigma_1 \geq \sigma_2 \quad (23)$$

Although analyzing this MM model is simply a matter of expanding the failure envelope in Fig. 2, it is still difficult to consider this failure criterion during TO. Because the envelopes in the second and forth quadrants are defined by the above four complex equations, it becomes complicated to introduce a unified differentiable equation for the MM model, further hindering effective TO.

2.3. Differentiability of the static failure criteria

As stated, because all of the static failure criteria – except for the DE criterion – are not differentiable with respect to both the principal stresses and the design variables, this section develops differentiable versions of these failure criteria.

2.3.1. MSS, DCM, BCM

In order to consider the above failure criteria – i.e., those from the MSS, DCM, and BCM theories – in stress-based topology optimization, the non-differentiable definitions with respect to the principal stress components must be substituted with differentiable definitions. In other words, as the maximum and minimum operators and the logical operator, *if*, are employed in their definitions, they need to be replaced by differentiable operators in order to complete the stress-based topology optimization with a gradient-based optimizer. To achieve this result, this paper introduces several operators that approximate these non-differentiable operators.

First, the pseudo-differentiable maximum and the minimum operators of the two arbitrarily real variables, a and b , can be defined such that

$$\Psi_{\max}(a, b) = \frac{a+b}{2} + \frac{\sqrt{(a-b)^2 + \varepsilon}}{2} \approx \begin{cases} a & a \geq b \\ b & a < b \end{cases} \quad (24)$$

$$\Psi_{\min}(a, b) = \frac{a+b}{2} - \frac{\sqrt{(a-b)^2 + \varepsilon}}{2} \approx \begin{cases} b & b \geq a \\ a & a < b \end{cases} \quad (25)$$

Note that the absolute operators have been replaced by the square root of a square with an infinitesimal epsilon addition, which effectively replaces the non-differentiable *absolute* operator in TO [8]. By combining the above operators, the following maximum and minimum operators for the three variables, a , b , and c , can be presented:

$$\begin{aligned} \tilde{\Psi}_{\max}(a, b, c) &= \frac{a}{4} + \frac{b}{4} + \frac{c}{2} + \frac{\sqrt{(a-b)^2 + \varepsilon}}{4} + \frac{\sqrt{\left(\frac{a}{2} + \frac{b}{2} - c + \frac{\sqrt{(a-b)^2}}{2}\right)^2 + \varepsilon}}{2} \\ &\approx \begin{cases} a & a \geq b \text{ and } a \geq c \\ b & b \geq a \text{ and } b \geq c \\ c & c \geq a \text{ and } c \geq b \end{cases} \end{aligned} \quad (26)$$

$$\begin{aligned} \tilde{\Psi}_{\min}(a, b, c) &= \frac{a}{4} + \frac{b}{4} + \frac{c}{2} - \frac{\sqrt{(a-b)^2 + \varepsilon}}{4} - \frac{\sqrt{\left(c - \frac{a}{2} - \frac{b}{2} + \frac{\sqrt{(a-b)^2}}{2}\right)^2 + \varepsilon}}{2} \\ &\approx \begin{cases} a & c \geq a \text{ and } b \geq a \\ b & c \geq b \text{ and } a \geq b \\ c & a \geq c \text{ and } b \geq c \end{cases} \end{aligned} \quad (27)$$

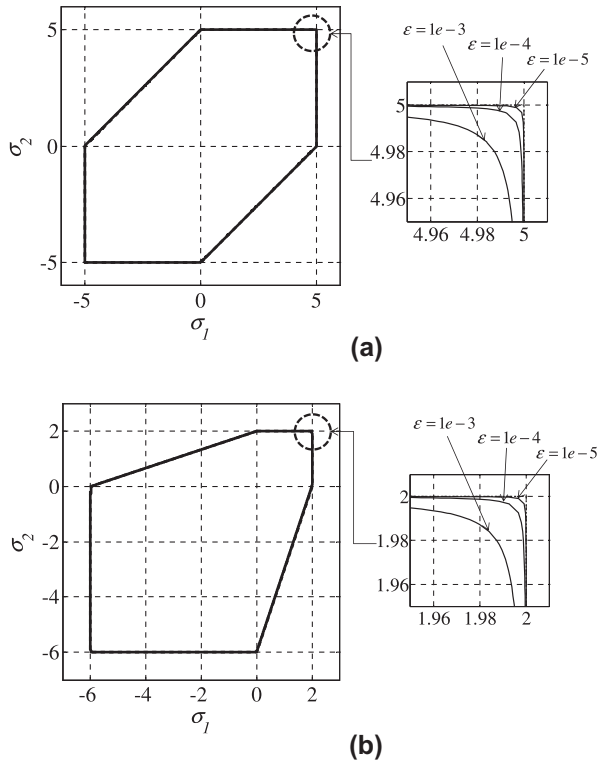


Fig. 3. The graphs of the failure envelopes as defined by the differentiable failure criteria for the plane stress element. (a) The failure envelope for the MSS theory and (b) the failure envelope for the DCM (or BCM) theory with $S_{yt}(S_{ut}) = 2$ and $S_{yc}(S_{uc}) = 6$.

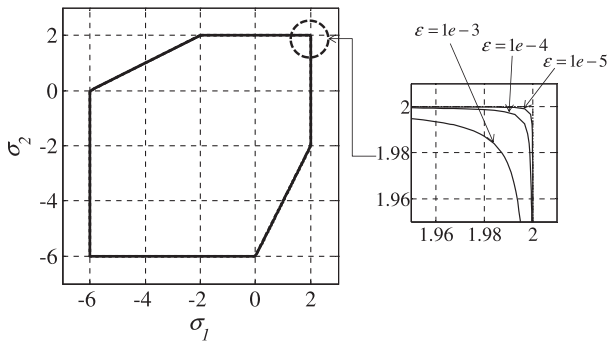


Fig. 4. The failure envelopes for both the original MM model and the present unified formulation with $S_{ut} = 2$ and $S_{uc} = 6$.

Owing to the epsilon value in the above formulations, the operators have different outputs depending on the order of the input variables. To remove this side effect, the average output values can be calculated with full permutation inputs:

$$\Psi_{\max}(a, b, c) = \frac{\tilde{\Psi}_{\max}(a, b, c) + \tilde{\Psi}_{\max}(a, c, b) + \tilde{\Psi}_{\max}(b, a, c) + \tilde{\Psi}_{\max}(b, c, a) + \tilde{\Psi}_{\max}(c, a, b) + \tilde{\Psi}_{\max}(c, b, a)}{6} \quad (28)$$

$$\Psi_{\min}(a, b, c) = \frac{\tilde{\Psi}_{\min}(a, b, c) + \tilde{\Psi}_{\min}(a, c, b) + \tilde{\Psi}_{\min}(b, a, c) + \tilde{\Psi}_{\min}(b, c, a) + \tilde{\Psi}_{\min}(c, a, b) + \tilde{\Psi}_{\min}(c, b, a)}{6} \quad (29)$$

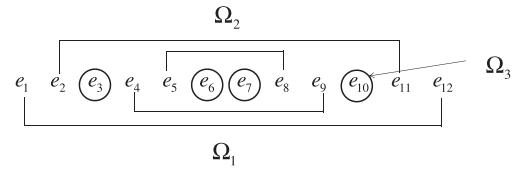


Fig. 5. A graphical description of the employed aggregation scheme developed in [42] ($RN = 3, NE = 12$). (the elements are sorted by according to the magnitude of stress.)

By utilizing the defined differentiable maximum and minimum operators for the three input values, the failure criteria of the MSS, DCM, and BCM theories can be redefined in differentiable forms as follows:

$$\text{The MSS theory : } g_e^{\text{MSS}} = \frac{\Psi_{\max}(\sigma_1, \sigma_2, \sigma_3)}{S_y} - \frac{\Psi_{\min}(\sigma_1, \sigma_2, \sigma_3)}{S_y} \leq 1 \quad (30)$$

$$\text{The DCM theory : } g_e^{\text{DCM}} = \frac{\Psi_{\max}(\sigma_1, \sigma_2, \sigma_3)}{S_t} - \frac{\Psi_{\min}(\sigma_1, \sigma_2, \sigma_3)}{S_c} \leq 1 \quad (31)$$

$$\text{The BCM theory : } g_e^{\text{BCM}} = \frac{\Psi_{\max}(\sigma_1, \sigma_2, \sigma_3)}{S_{ut}} - \frac{\Psi_{\min}(\sigma_1, \sigma_2, \sigma_3)}{S_{uc}} \leq 1 \quad (32)$$

In Fig. 3, the approximated curves are drawn for various epsilons. As shown, the above formulations are close enough to be employed as substitutes for the original envelopes of the MSS theory and the DCM (or BCM) theory.

2.3.2. A unified MM theory

Because the logical operator, *if*, is used to define the envelopes in the second and forth quadrants of the MM failure criterion, it becomes more complicated from a numerical perspective. In order to derive one unified criterion for the MM theory, this paper presents a new idea that will now be described. First, the failure criterion in (22) can be represented as (33) by dividing the numerator of the first term of (22) such that

$$\frac{\sigma_1}{S_{ut}} - \frac{\sigma_2}{S_{uc}} - \frac{\sigma_1}{S_{uc}} \leq 1 \quad (33)$$

Note that the difference between (32) and (33) is the third term of the left side of (33) and the condition $|\frac{\sigma_2}{\sigma_1}| > 1$ in (22) can be changed to (34):

$$0 > -\sigma_1 > \sigma_2 \quad (34)$$

Moreover, note that the third term in (33) is the second largest value among the values 0 , $-\sigma_1/S_{uc} (= -\max(\sigma_1, \sigma_2, 0)/S_{uc})$, and $\sigma_2/S_{uc} (= \min(\sigma_1, \sigma_2, 0)/S_{uc})$. Consequently, since this rule is applicable for the equations from (20) to (23), the following unified formulation for the MM theory can be obtained:

$$g_e^{\text{MM}} = \frac{\Psi_{\max}(\sigma_1, \sigma_2, 0)}{S_{ut}} - \frac{\Psi_{\min}(\sigma_1, \sigma_2, 0)}{S_{uc}} + \frac{\Psi_2(0, -\Psi_{\max}(\sigma_1, \sigma_2, 0), \Psi_{\min}(\sigma_1, \sigma_2, 0))}{S_{uc}} \leq 1 \quad (35)$$

$$\Psi_2(a, b, c) = a + b + c - \Psi_{\max}(a, b, c) - \Psi_{\min}(a, b, c) \quad (36)$$

where $\Psi_2(a, b, c)$ is the differentiable operator providing the second largest value among the three inputs. (See the appendix for a more detailed numerical derivation.)

Fig. 4 shows the envelope of the approximated MM failure criterion (35) for the plane stress element. As this figure illustrates, it is possible to define an envelope sufficiently close to the original envelope.

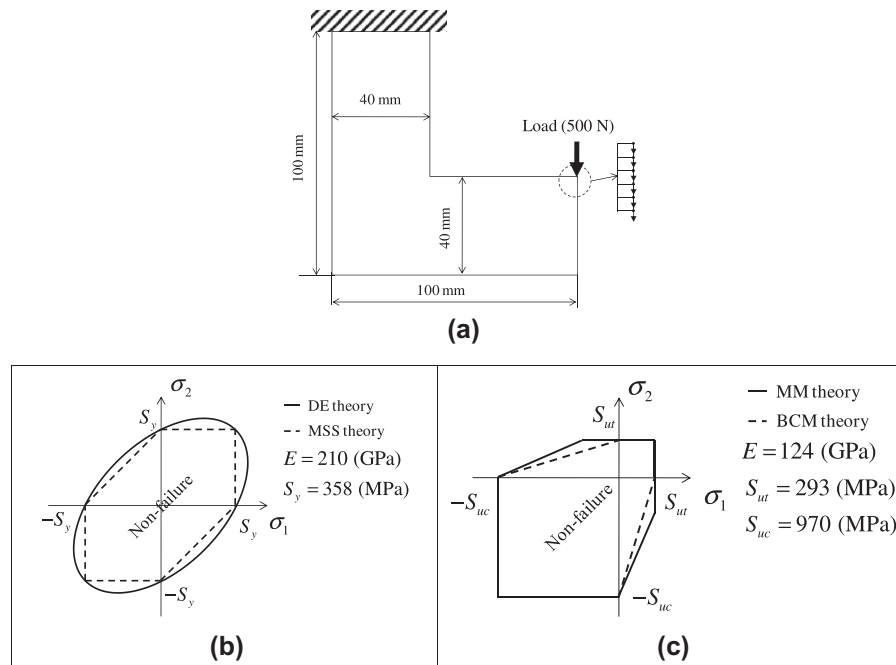


Fig. 6. An L-shaped beam structure: (a) the geometry (The external load, 500 N, was distributed on the six nodes of the tip of the right edge, $\nu = 0.3$, the number of QUAD element: 6400) (b) the material properties and the failure envelopes for the DE and MSS theories for carbon steel 1018, and (c) the material properties and the failure envelopes for the BCM and MM theories for ASTM A48 gray iron 40.

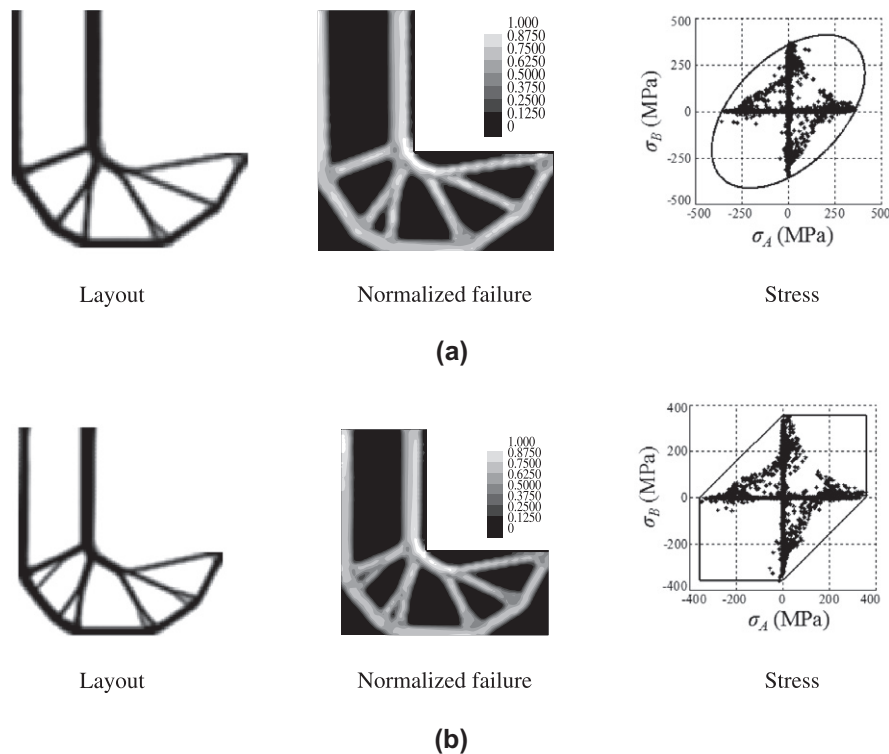


Fig. 7. The optimized layouts of the L-shaped beam with the DE theory and the MSS theory ($RN = 8, n = 3$ and $n_s = 0.5, \sigma_A$ and σ_B : unsorted principal stresses). (a) The layout using the DE theory ($V/V_0 = 0.293$) and (b) the layout using the MSS theory ($V/V_0 = 0.323$).

2.4. An aggregation scheme of design domain

For a robust TO procedure, it is essential to employ an aggregation scheme that divides a design domain into several subdomains, called *regions*, in order to evaluate the constraints in (9). Previous

research that utilized this design domain segregation scheme [27–29] reported that it was necessary to consider the oscillations of element-wise stress values. This paper addresses the two known variations, namely, a scheme based on the graphical location and a scheme based on a sorting algorithm, and employs the latter – an

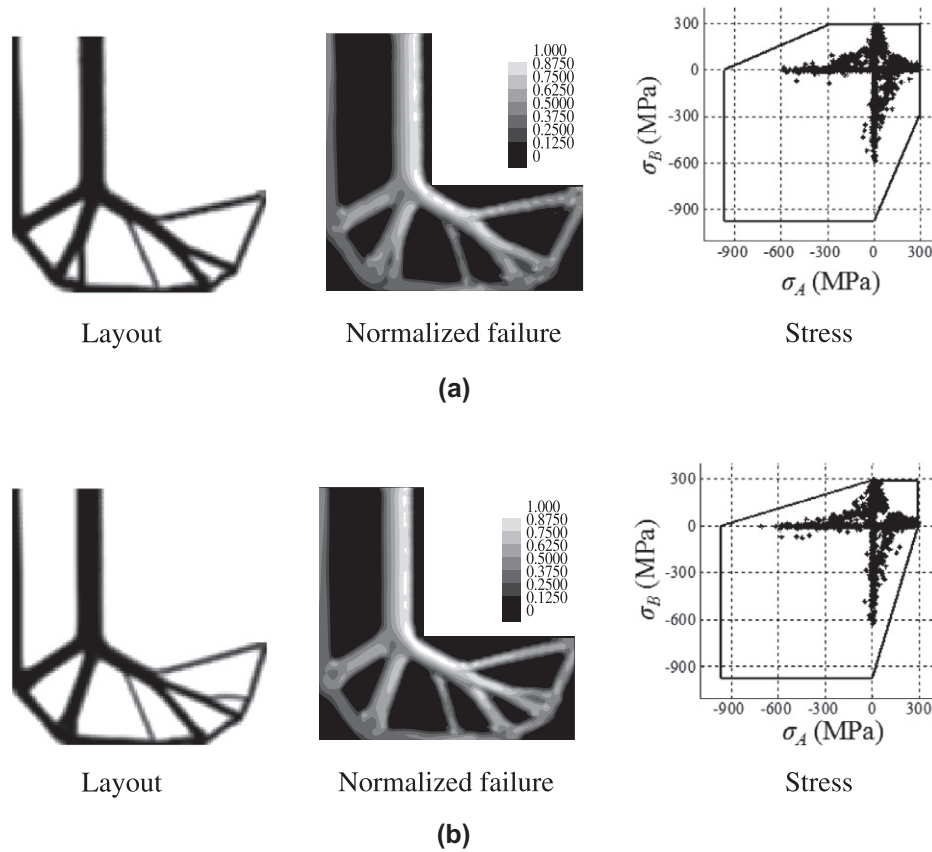


Fig. 8. The optimized layouts of the L-shaped beam with the MM theory and the BCM theory ($RN = 8, n = 3$ and $n_s = 0.5$) (a) The layout using the MM theory ($V/V_0 = 0.354$) and (b) the layout using the BCM theory ($V/V_0 = 0.356$).

aggregation algorithm developed in [42]¹ and based on the sorting algorithm contributed by the authors.

First, the finite elements are sorted according to the magnitude of their stress constraint functions, and the k th region of the RN regions is defined as

$$\Omega_k \equiv \{e_k, e_{RN+k}, \dots, e_{NE/2-(RN-k)}, e_{NE/2+(RN-k)+1}, \dots, e_{NE-(RN+k)+1}, e_{NE-k+1}\} \quad (k = 1, 2, \dots, RN) \quad (37)$$

For the case with $RN = 3$ and $NE = 12$, the three regions are defined as follows:

$$\begin{aligned} \Omega_1 &\equiv \{e_1, e_4, e_9, e_{12}\} \\ \Omega_2 &\equiv \{e_2, e_5, e_8, e_{11}\} \\ \Omega_3 &\equiv \{e_3, e_6, e_7, e_{10}\} \end{aligned} \quad (38)$$

A graphical description of the proposed segregation scheme is given in Fig. 5.

3. Numerical examples

In this section, the three numerical topology optimization problems (an L-shaped bracket, a cantilever beam, and a three-dimensional beam) are solved to show the validity and utility of the present topology optimization method for static failure criteria. Real material properties are implemented, but in order to show the

effects of strength changes, some artificial values are also employed. Moreover, in order to solve the optimization problem, the method of moving asymptotes (MMA) [43] is used. Due to the local optima issues in structural topology optimization, the present designs are not the global optima. (See [7] and references therein for the local optima issue) For the convergence criteria, the maximum change of design variables between two sequential optimization iterations is considered, and the maximum optimization iteration is fixed to 1000.

3.1. Example: 1 L-bracket

For the first numerical example, we consider an L-shaped beam with a fixed upper edge and a vertical load applied to the right middle, as shown in Fig. 6(a). This example has been widely used by many previous STOM research efforts [27–29]. Because it has a reentrant corner where stress concentration occurs, comparisons of the topological changes between optimized layouts by minimizing compliance and constraining stress with (39) can be made. To test the MSS and DE theories, the material properties of carbon steel 1018, a ductile metal, were utilized. Likewise, to test the BCM and MM theories, the material properties of the ASTM A48 gray iron 40, a brittle metal, were employed [41]. Because the BCM and the DCM theories share the same mathematical formulation, only the BCM theory was tested here. The detailed geometry and material properties are given in Fig. 6, and the graphical illustrations of the failure envelopes for each criterion are given in Fig. 6(b) and (c). For the plane stress analysis, the bilinear QUAD elements (1.0 mm by 1.0 mm) were used to discretize the design domain, and the center stress of each element was evaluated for

¹ The research in [42] Jeong SH, Choi DH, Yoon GH. Separable stress interpolation scheme for stress-based topology optimization with multiple materials. in review 2011 presents the separable stress interpolation scheme for the continuum topology optimization with multiple materials only considering the DE theory.

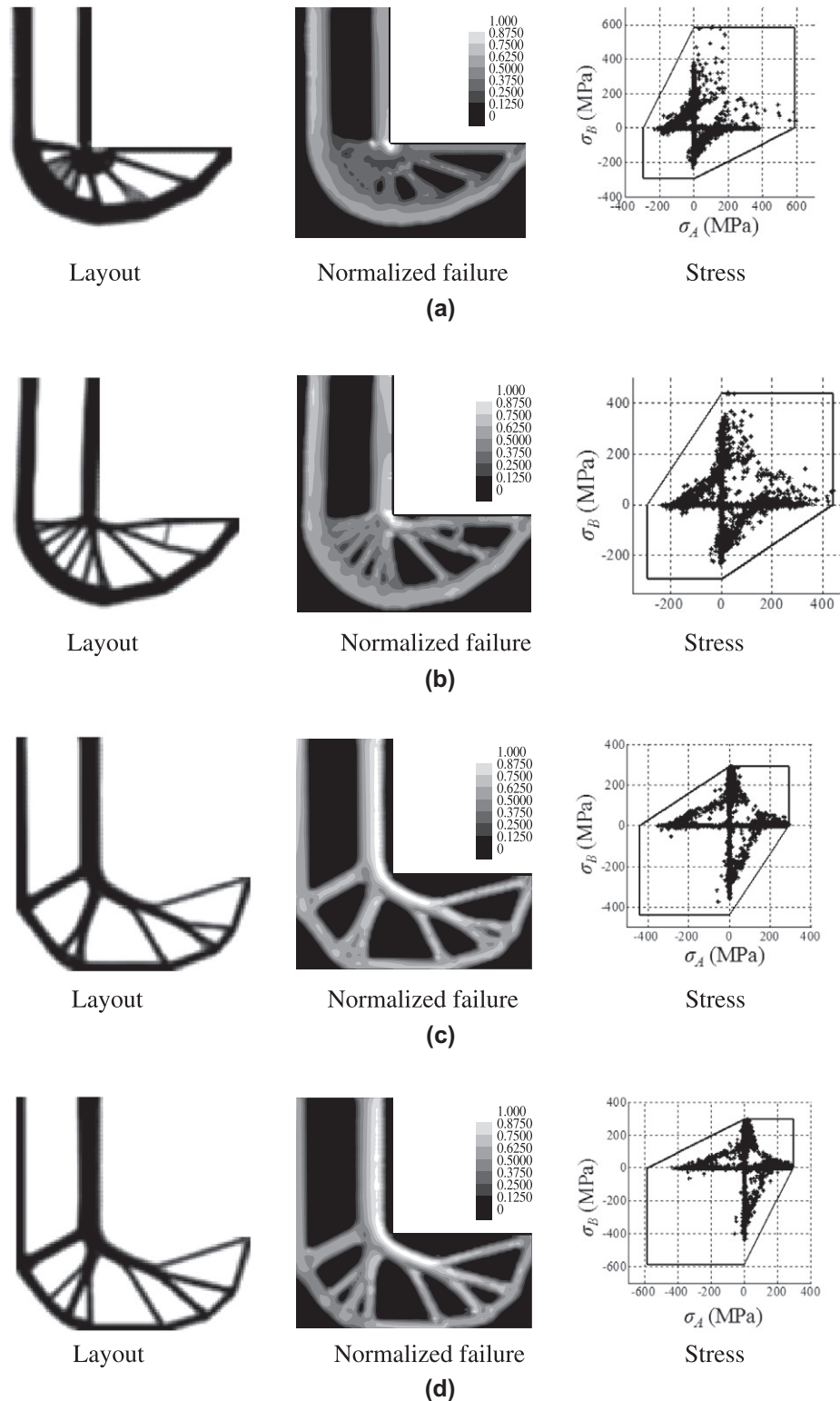


Fig. 9. The optimized layout of a cantilever beam according to the ratios between S_{ut} and S_{uc} using BCM theory: (a) $S_{ut}:S_{uc} = 2:1$, (b) $S_{ut}:S_{uc} = 1.5:1$, (c) $S_{ut}:S_{uc} = 1:1.5$, and (d) $S_{ut}:S_{uc} = 1:2$ ($RN = 8$, $n = 3$ and $n_s = 0.5$).

the static failure criteria. For the regulation of the design process, the filtering radius was set to three times the element size. The number of subdomains RN was fixed to eight for this example. Figs. 7 and 8 show the optimized topology layouts for each failure criterion. The contours of normalized failures (30)–(32), (35), which all should be less than one, are also represented. At the cor-

ner, the smooth boundaries appear to minimize stress concentrations in both layouts, as expected. Because the MSS theory is more conservative than the DE theory with similar envelopes, the mass usage by the MSS failure criterion was larger than that by the DE failure criterion (see Fig. 7). Fig. 8(a) and (b) show the results of the tests using the BCM and MM theories with the mate-

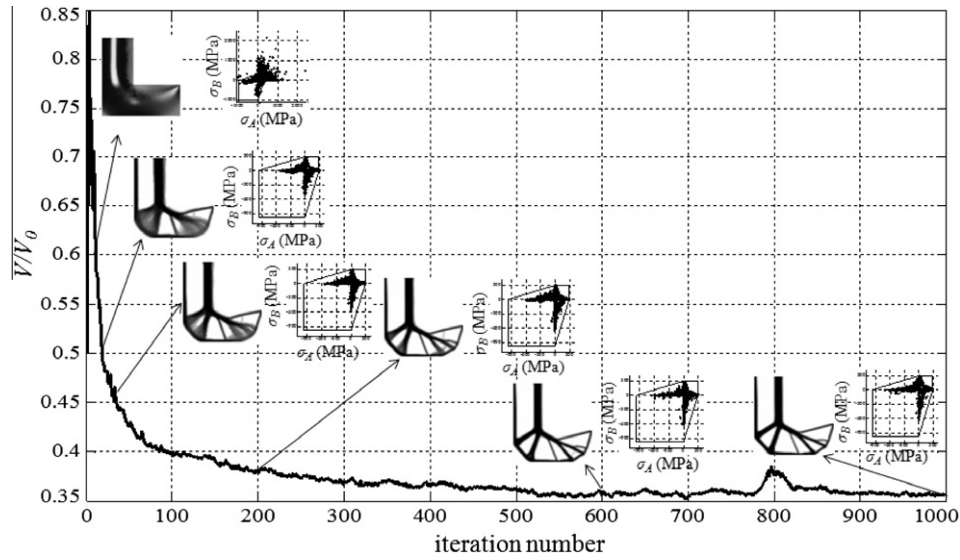


Fig. 10. Intermediate layout designs of Fig. 8(b).

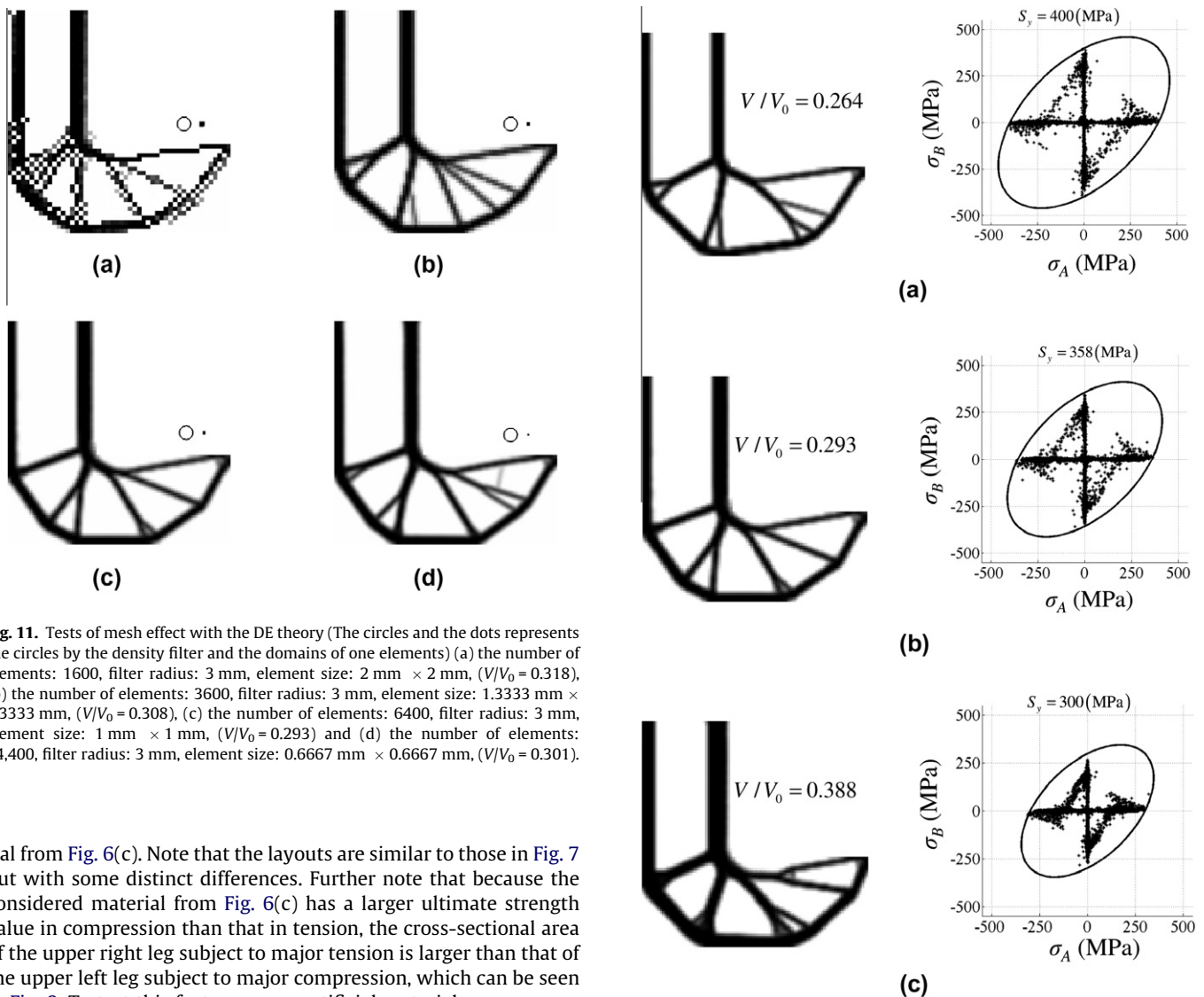


Fig. 11. Tests of mesh effect with the DE theory (The circles and the dots represents the circles by the density filter and the domains of one elements) (a) the number of elements: 1600, filter radius: 3 mm, element size: 2 mm \times 2 mm, ($V/V_0 = 0.318$), (b) the number of elements: 3600, filter radius: 3 mm, element size: 1.3333 mm \times 1.3333 mm, ($V/V_0 = 0.308$), (c) the number of elements: 6400, filter radius: 3 mm, element size: 1 mm \times 1 mm, ($V/V_0 = 0.293$) and (d) the number of elements: 14,400, filter radius: 3 mm, element size: 0.6667 mm \times 0.6667 mm, ($V/V_0 = 0.301$).

rial from Fig. 6(c). Note that the layouts are similar to those in Fig. 7 but with some distinct differences. Further note that because the considered material from Fig. 6(c) has a larger ultimate strength value in compression than that in tension, the cross-sectional area of the upper right leg subject to major tension is larger than that of the upper left leg subject to major compression, which can be seen in Fig. 8. To test this feature, some artificial materials were examined by changing the ratios of the ultimate strength value in

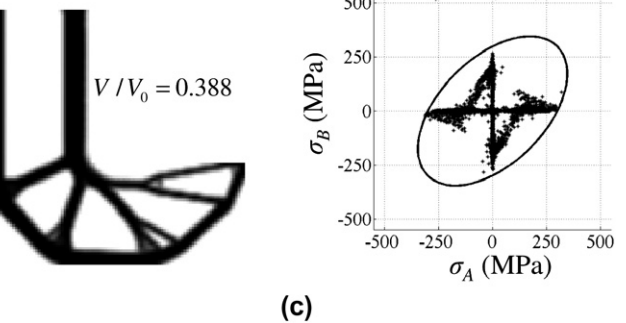


Fig. 12. The effect of the different yield stress values of the DE theory.

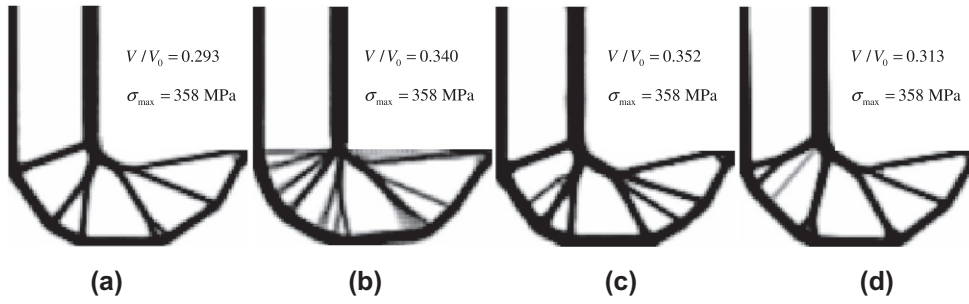


Fig. 13. Tests of different penalization parameters (n and n_s) with the DE theory: (a) $n = 3$, $n_s = 0.5$ (b) $n = 3$, $n_s = 1.0$ (c) $n = 4$, $n_s = 0.5$ and (d) $n = 4$, $n_s = 1.0$.

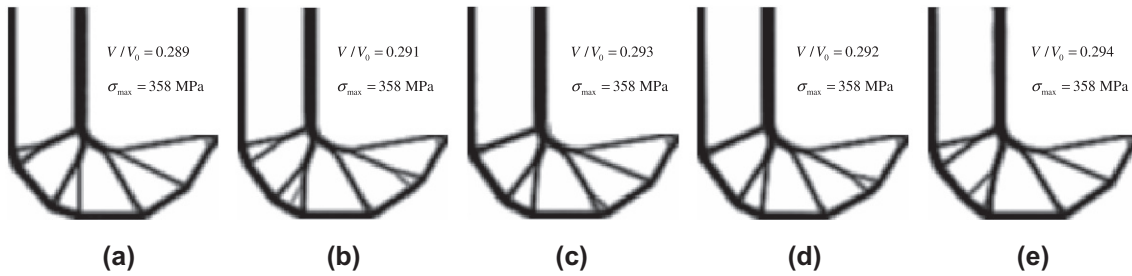


Fig. 14. The numerical investigations of the damping factor (α) with the DE theory: (a) $\alpha = 0.1$ (b) $\alpha = 0.3$ (c) $\alpha = 0.5$ (d) $\alpha = 0.7$ and (e) $\alpha = 0.9$.

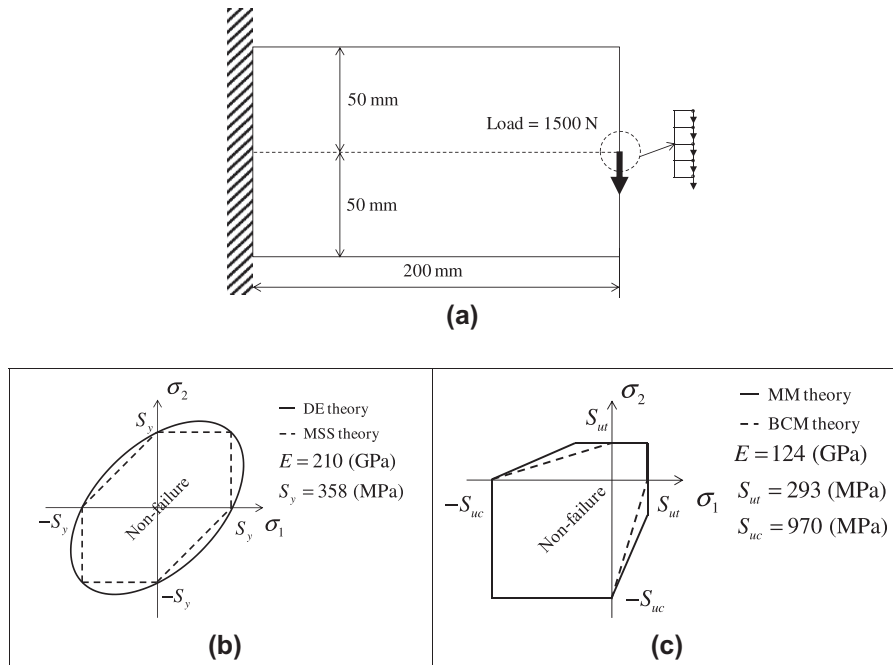


Fig. 15. A cantilever beam structure: (a) the geometry (The external load, 1500 N, was distributed on the five nodes at the tip of the right center edge, $\nu = 0.3$, the number of QUAD elements: 5000), (b) the material properties and the failure envelopes for the DE and MSS theories for carbon steel 1018, and (c) the material properties and the failure envelopes for the BCM and MM theories for ASTM A48 gray iron 40.

compression to that of the value in tension, which can be seen in Fig. 9. Since the BCM theory is more conservative than the MM theory, the BCM model used more mass than the MM model, as was similarly observed in the ductile material. Furthermore, all stresses are inside the approximated envelopes. Fig. 10 shows the intermediate layouts and the convergence history from throughout the topology optimization. Due to the density filter, some oscillations were observed, and around the 800th iteration, some large oscillations were observed because a small beam near or at the loading point disappeared.

$$\text{Minimize}_{\gamma} V(\tilde{\gamma}) = \sum_{e=1}^{NE} \tilde{\gamma}_e v_e \quad (\tilde{\gamma} : \text{Filtered density})$$

$$\text{subject to } \langle g_{\max} \rangle_1 \leq 1$$

$$\langle g_{\max} \rangle_2 \leq 1$$

$$\vdots$$

$$\langle g_{\max} \rangle_{RN} \leq 1$$

$$\tilde{\gamma} = \Xi(\gamma) \quad \text{with the density filter } \Xi$$

(39)

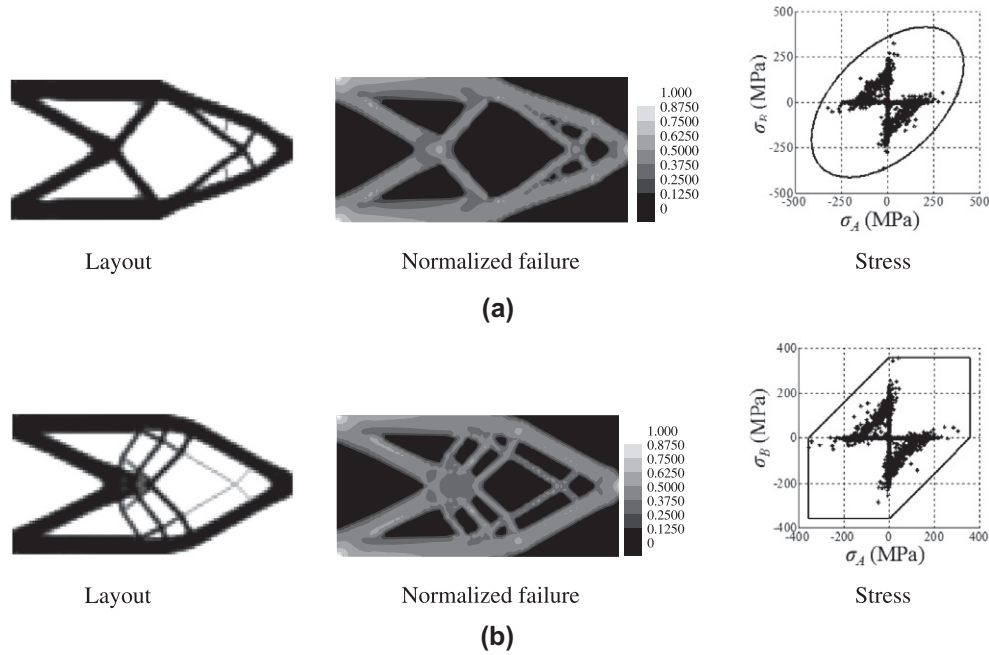


Fig. 16. The optimized layouts of the cantilever beam with the DE theory and the MSS theory ($RN = 4, n = 3$ and $n_s = 0.5$). (a) The layout with the DE theory ($V/V_0 = 0.410$) and (b) the layout with the MSS theory ($V/V_0 = 0.433$).

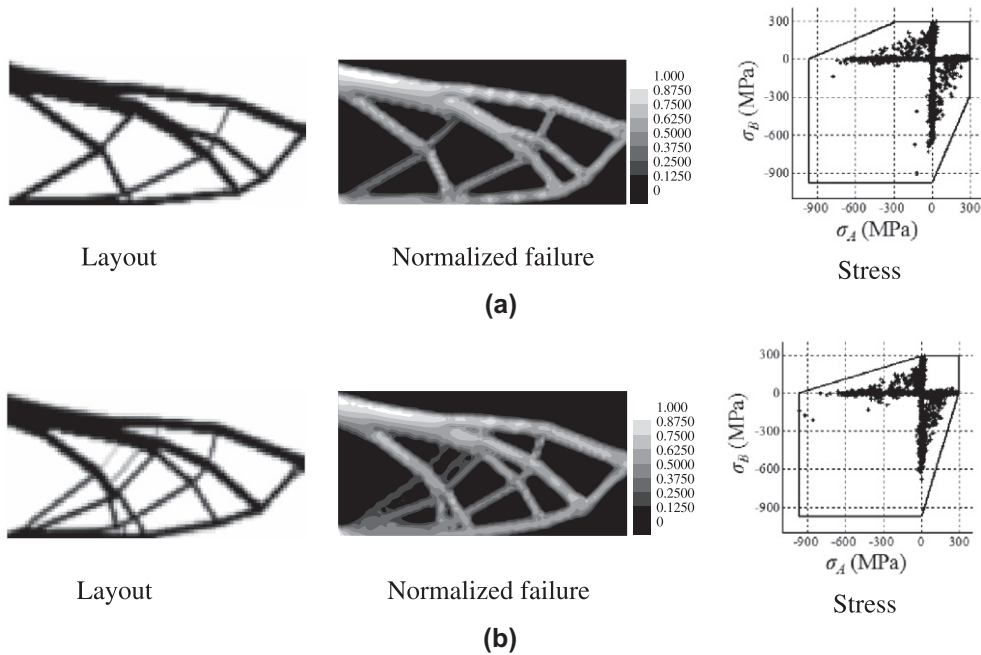


Fig. 17. The optimized layouts of the cantilever beam with the MM theory and the BCM theory ($RN = 4, n = 3$ and $n_s = 0.5$). (a) The layout with the MM theory ($V/V_0 = 0.295$) and (b) the layout with the BCM theory ($V/V_0 = 0.306$).

As it is an important aspect to see the effect of the mesh-refinement in topology optimization, Fig. 11 shows some optimized layouts with various FE meshes with a fixed density filter (radius = 3 mm). The size of element being large compared with that of the filter in Fig. 11(a), the filter does not work as expected. In Fig. 11(a)–(d), although some differences in detail are observed at the inside of the outer structures, the other parts are similar to each other. Some differences are due to the local optima problem in topology optimization. We also investigate the effects of the different yield stress values in Fig. 12 with the DE theory. By decreasing the limit stress

value into 300 MPa, the optimized layout with 38.8% mass usage is used in Fig. 12(c). As expected, the structural members become thicker. On the other hand, with the higher limit stress value (400 MPa), the optimized layout of Fig. 12(a) with 26.4% mass usage is obtained. As shown, the thinner members appear.

We also investigate the effects of the penalization parameters (n and n_s) in Fig. 13. It is general to use 3 or 4 for n to penalize intermediate design variables and a lower value should be used for n_s used for the stress evaluation to avoid the stress singularity problem. According to our investigations, with a smaller value of n_s , the

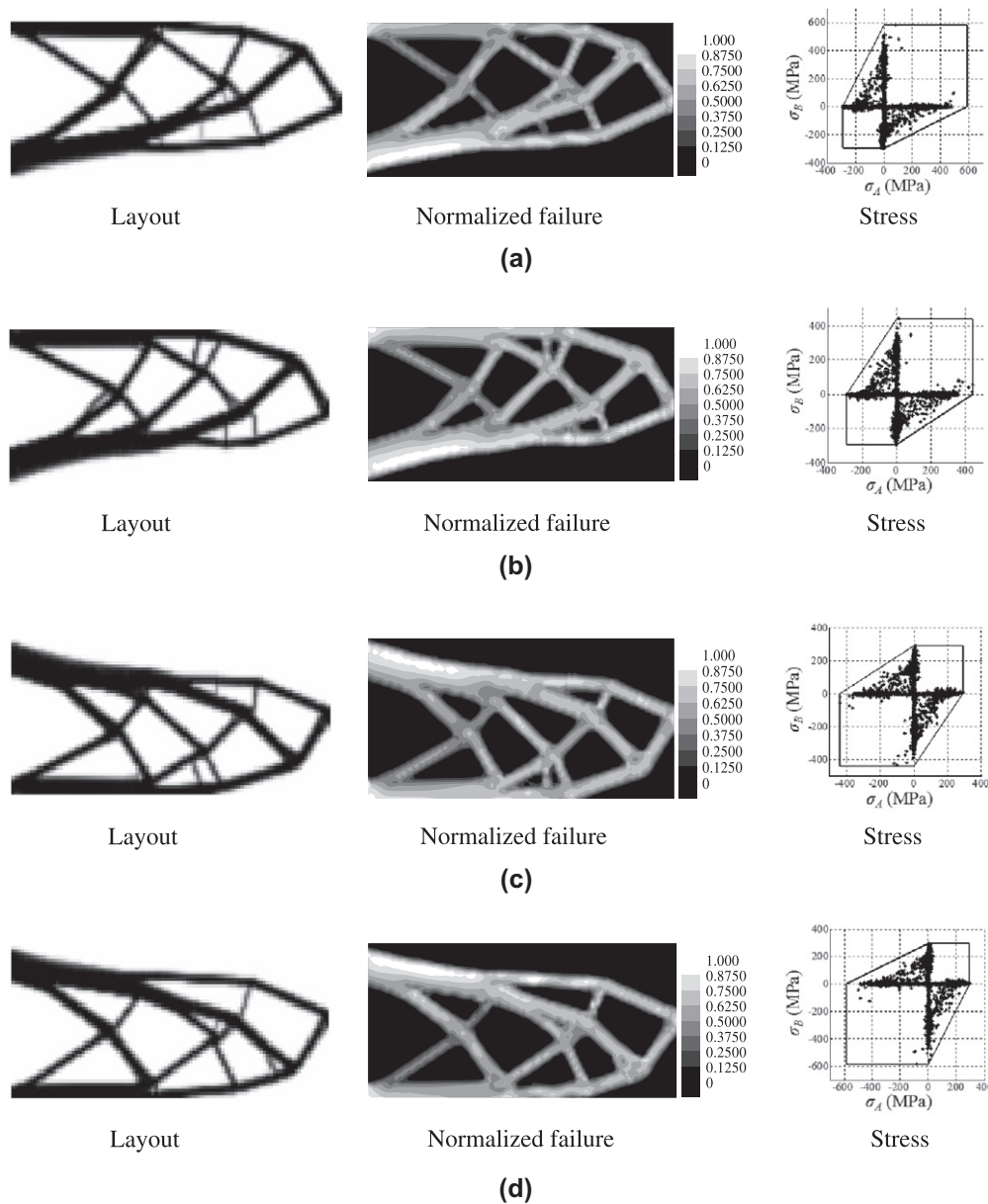


Fig. 18. The optimized layouts of the cantilever beam with various ratios between S_{ut} and S_{uc} using BCM theory: (a) $S_{ut}:S_{uc} = 2:1$, (b) $S_{ut}:S_{uc} = 1.5:1$, (c) $S_{ut}:S_{uc} = 1:1.5$, and (d) $S_{ut}:S_{uc} = 1:2$ ($RN = 4$, $n = 3$ and $n_s = 0.5$).

larger curvatures in the entrance corner are appeared. This is because the stress values of intermediate densities are further penalized. In addition, we investigate the effects of damping parameter α in Fig. 14. According to our numerical investigations, with the different values of α , we obtain the local optimal layouts.

3.2. Example 2: cantilever beam example

For the second numerical example, a cantilever beam (200 mm by 100 mm) was optimized using the same materials from the first numerical example. First, it was discretized by 5000 plane stress elements, as shown in Fig. 15. The optimized layouts for the various static failure theories are compared to each other in Figs. 16 and 17. Because the failure envelopes from the DE theory and the MSS theory were symmetric, the symmetric designs in Fig. 16 could be obtained. As in the previous example, the mass usage by the MSS theory was higher than that by the DE theory.

In the result of Fig. 16(b), some thin members with intermediate design variables are observed. They are inevitable due to the density filtering and the relaxed stress values of these members are below the stress constraint. However, some other measures should be considered in the optimization formulation in order to remove these thin and grey members. Furthermore, the shape optimization process should be used in our opinion.

However, Fig. 17 shows the non-symmetric layouts from the BCM and MM theories. Because the ultimate compression strength is greater than the ultimate tension strength, the optimized layouts have more mass distributed in the upper part of the layout, which is under tension. For the purpose of this investigation, Fig. 18 shows the optimized layouts that are a result of changing the ratio of the ultimate compression strength to the ultimate tension strength. As the ratio varies, changes in the mass distribution from the upper part of the layout to the lower part can be observed. This example demonstrates that, when using materials with different tension and compression yield strengths, it is better to use a

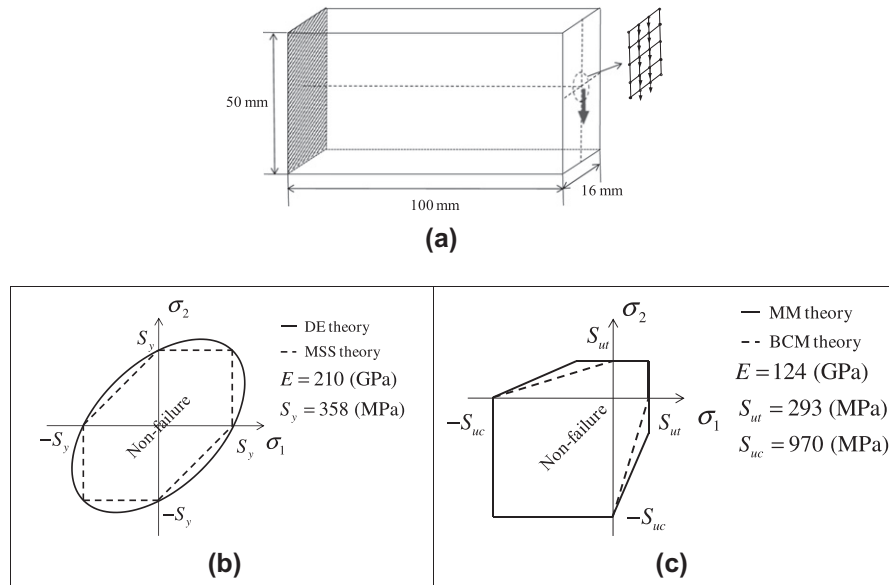


Fig. 19. A three-dimensional cantilever beam structure: (a) the geometry (The external load, 1200 N, was distributed on the ten nodes of the tip of the right center edge, $\nu = 0.3$, the number of Hexagonal elements: 40,000), (b) the material properties and the failure envelopes for the DE and MSS theories for carbon steel 1018, and (c) and the material properties and the failure envelopes for the BCM and MM theories for ASTM A48 gray iron 40.

non-symmetric design, even with linear strain and symmetric loading mechanical conditions.

3.3. Example 3: 3-Dimensional cantilever beam

For the last example, a three-dimensional cantilever beam (100 mm by 50 mm by 16 mm) was considered, and is shown in Fig. 19. The distributed mechanical load in Fig. 19(a) was applied to the ten nodes on the center-of-right face; the end of the beam was fixed. Only half of the design domain was solved; even with the effects from the material properties, the design symmetry at the plane with the symmetric boundary condition had to be maintained. The material properties and the optimization parameters are listed in Fig. 19.

The optimized layouts obtained by imposing the DE, MSS, MM, and BCM theories in TO are presented in Fig. 20. All of the imposed constraints were satisfied and converged. As observed in the two-dimensional examples, symmetric designs were obtained with the DE and MSS theories while asymmetric designs were obtained with the MSS and BCM theories. Moreover, the designs from the MSS and BCM theories were prone to have more mass, which was also observed in the two-dimensional examples.

4. Conclusions

This research presented a new topology optimization framework that considered various failure criteria, including the DE theory, the MSS theory, the DCM theory, the BCM theory, and the MM theory, by introducing a differentiable maximum and minimum operator as well as a differentiable logical operator. These operators were essential for deriving the sensitivity analysis of these failure criteria with respect to both the topology optimization design variables and the principal stress values. By solving several two- and three-dimensional numerical examples, the following conclusions can be made:

1. Even with a symmetric design domain, symmetric boundary conditions (load and displacement), and a symmetric linear material, non-symmetric designs should be used with materials

that have different compression and tensile strengths; it has been researched that with different Young's moduli or stress limits for tension and compression, asymmetrical designs can be obtained (See [33–35] and reference therein). In our research, we confirm that with the same Young's modulus for tension and compression but with different failure limits, asymmetrical continuum layouts can be used with various static failure criteria for ductile or brittle material. This conclusion is one of the main findings of this research.

2. With the developed topology optimization framework, this research showed that it is now possible to consider the various static failure criteria in the two- and three-dimensional TO. In addition, observations indicated that more conservative failure criteria, e.g., the MSS theory for ductile material and the BCM theory for brittle material, utilized more mass, as was expected.
3. Although some uncertainties remain because of the presence of the density filter, this research demonstrated that it is possible for topology optimization to ascertain the optimized topological layouts – i.e., the local optima – by constraining the various static failure criteria. Furthermore, by changing the compression or tensile strengths, it showed that it is possible to change some of the configuration details such as the cross-sectional area and smooth corners. However, in our opinion, the shape optimization process should be incorporated after applying the developed topology optimization procedure.
4. Despite all of the other research in this field, including this research, the dynamic failure criteria (i.e., fatigue) has not yet been considered for TO. These criteria need to be the focus of future research, not only for academic test structures but also for implementation in practical engineering structures. Some of the numerical techniques developed in this research may be applicable for this purpose.

In conclusion, this research developed and tested a new topology optimization process that considered the various static failure criteria for the first time and demonstrated the validity and potential of the present approach by solving two- and three-dimensional topology optimization problems.

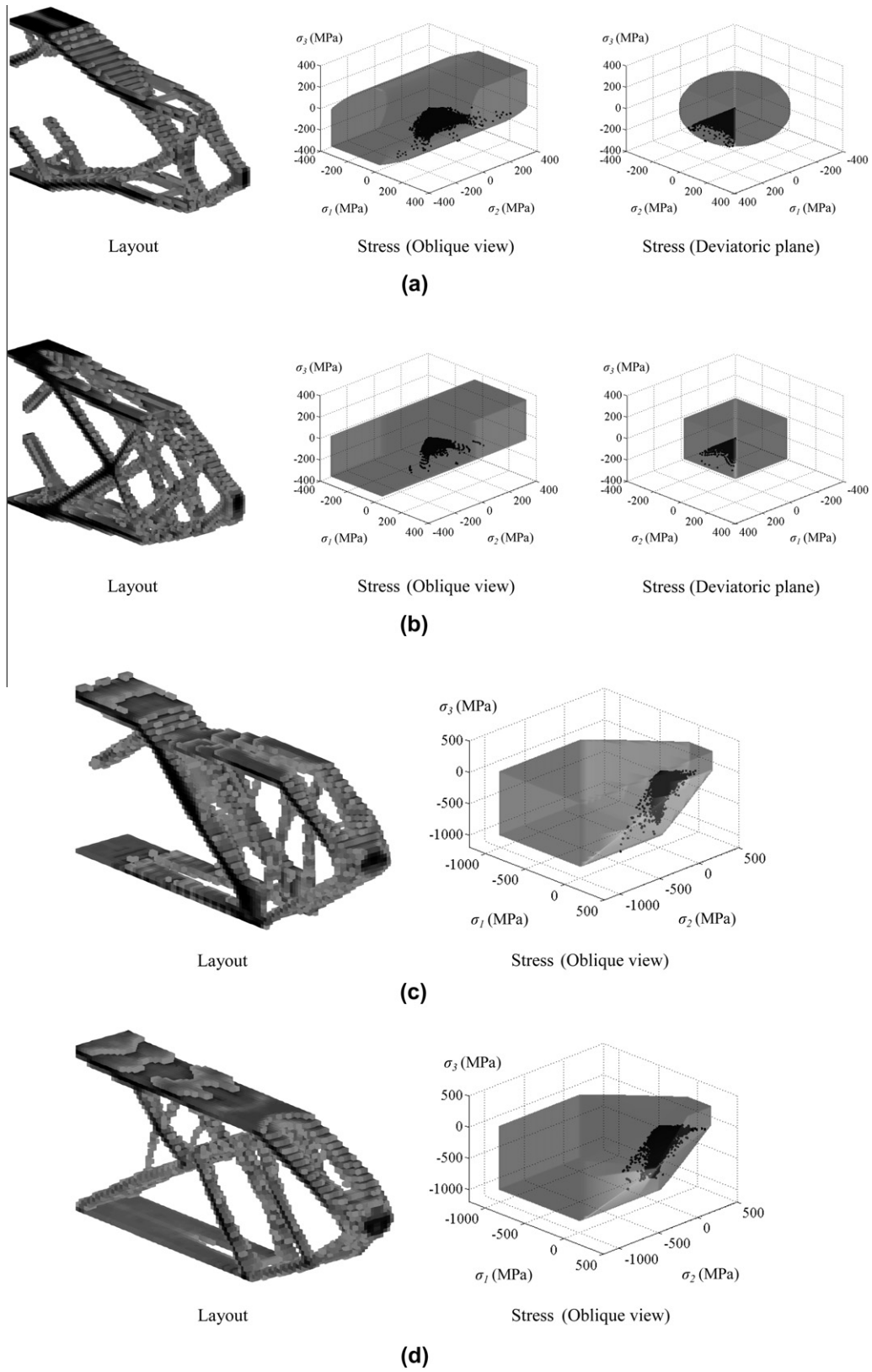


Fig. 20. The oblique views of the optimized layouts with (a) the DE theory ($\frac{\nu}{\nu_0} = 0.103$), (b) the MSS theory ($\frac{\nu}{\nu_0} = 0.136$), (c) the MM theory ($\frac{\nu}{\nu_0} = 0.105$), and (d) the BCM theory ($\frac{\nu}{\nu_0} = 0.109$) (The gray surfaces represent the envelopes of the failure criteria).

Appendix A. The unified criterion for the MM

The applicability of the proposed differentiable criterion for the MM theory is verified for the four cases of MM theory as follows:

(i) If $\sigma_1 \geq \sigma_2 \geq 0$

$$\begin{aligned} & \frac{\Psi_{\max}(\sigma_1, \sigma_2, 0)}{S_{ut}} - \frac{\Psi_{\min}(\sigma_1, \sigma_2, 0)}{S_{uc}} \\ & - \frac{\Psi_2(0, -\Psi_{\max}(\sigma_1, \sigma_2, 0), \Psi_{\min}(\sigma_1, \sigma_2, 0))}{S_{uc}} \\ & = \frac{\sigma_1}{S_{ut}} - \frac{0}{S_{uc}} + \frac{0+0-\sigma_1}{S_{uc}} - \frac{\max(-\sigma_1, 0, 0)}{S_{uc}} \\ & - \frac{\min(-\sigma_1, 0, 0)}{S_{uc}} = \frac{\sigma_1}{S_{ut}} + \frac{0+0-\sigma_1}{S_{uc}} \\ & - 0 - \frac{-\sigma_1}{S_{uc}} = \frac{\sigma_1}{S_{ut}} \geq 1 \end{aligned} \quad (40)$$

(ii) If $\sigma_1 \geq 0 \geq \sigma_2$ and $\left|\frac{\sigma_2}{\sigma_1}\right| \leq 1$

$$\begin{aligned} & \frac{\Psi_{\max}(\sigma_1, \sigma_2, 0)}{S_{ut}} - \frac{\Psi_{\min}(\sigma_1, \sigma_2, 0)}{S_{uc}} \\ & - \frac{\Psi_2(0, -\Psi_{\max}(\sigma_1, \sigma_2, 0), \Psi_{\min}(\sigma_1, \sigma_2, 0))}{S_{uc}} \\ & = \frac{\sigma_1}{S_{ut}} - \frac{\sigma_2}{S_{uc}} + \frac{0+\sigma_2-\sigma_1}{S_{uc}} - \frac{\max(-\sigma_1, \sigma_2, 0)}{S_{uc}} \\ & - \frac{\min(-\sigma_1, \sigma_2, 0)}{S_{uc}} = \frac{\sigma_1}{S_{ut}} - \frac{\sigma_2}{S_{uc}} + \frac{\sigma_2-\sigma_1}{S_{uc}} - \frac{0}{S_{uc}} - \frac{-\sigma_1}{S_{uc}} \\ & = \frac{\sigma_1}{S_{ut}} - \frac{\sigma_2}{S_{uc}} + \frac{\sigma_2-\sigma_1}{S_{uc}} - \frac{-\sigma_1}{S_{uc}} = \frac{\sigma_1}{S_{ut}} \geq 1 \end{aligned} \quad (41)$$

(iii) If $\sigma_1 \geq 0 \geq \sigma_2$ and $\left|\frac{\sigma_2}{\sigma_1}\right| > 1$

$$\begin{aligned} & \frac{\Psi_{\max}(\sigma_1, \sigma_2, 0)}{S_{ut}} - \frac{\Psi_{\min}(\sigma_1, \sigma_2, 0)}{S_{uc}} \\ & - \frac{\Psi_2(0, -\Psi_{\max}(\sigma_1, \sigma_2, 0), \Psi_{\min}(\sigma_1, \sigma_2, 0))}{S_{uc}} \\ & = \frac{\sigma_1}{S_{ut}} - \frac{\sigma_2}{S_{uc}} + \frac{\sigma_2-\sigma_1}{S_{uc}} - \frac{\max(-\sigma_1, \sigma_2, 0)}{S_{uc}} \\ & - \frac{\min(-\sigma_1, \sigma_2, 0)}{S_{uc}} = \frac{\sigma_1}{S_{ut}} - \frac{\sigma_2}{S_{uc}} + \frac{\sigma_2-\sigma_1}{S_{uc}} - \frac{0}{S_{uc}} - \frac{\sigma_2}{S_{uc}} \\ & = \frac{\sigma_1}{S_{ut}} - \frac{\sigma_1}{S_{uc}} - \frac{\sigma_2}{S_{uc}} \geq 1 \end{aligned} \quad (42)$$

(iv) If $0 \geq \sigma_1 \geq \sigma_2$

$$\begin{aligned} & \frac{\Psi_{\max}(\sigma_1, \sigma_2, 0)}{S_{ut}} - \frac{\Psi_{\min}(\sigma_1, \sigma_2, 0)}{S_{uc}} \\ & - \frac{\Psi_2(0, -\Psi_{\max}(\sigma_1, \sigma_2, 0), \Psi_{\min}(\sigma_1, \sigma_2, 0))}{S_{uc}} \\ & = \frac{0}{S_{ut}} - \frac{\sigma_2}{S_{uc}} + \frac{\sigma_2-0}{S_{uc}} - \frac{\max(-0, \sigma_2, 0)}{S_{uc}} - \frac{\min(-0, \sigma_2, 0)}{S_{uc}} \\ & = -\frac{\sigma_2}{S_{uc}} + \frac{\sigma_2-0}{S_{uc}} - \frac{0}{S_{uc}} - \frac{\sigma_2}{S_{uc}} = -\frac{\sigma_2}{S_{uc}} \geq 1 \end{aligned} \quad (43)$$

Appendix B. Sensitivity analysis of the p-norm stress with respect to design variables

To conduct the present stress-based topology optimization with a gradient-based optimizer, the sensitivity of the p -norm of the failure criteria with respect to the design variables should be derived. First, the sensitivity value of the p -norm of the failure criteria can be derived as follows.

$$\begin{aligned} \frac{d\langle\sigma_{PN}\rangle_k}{d\tilde{\gamma}_e} &= \frac{\partial\langle\sigma_{PN}\rangle_k}{\partial\tilde{\gamma}_e} + \frac{\partial\langle\sigma_{PN}\rangle_k}{\partial\mathbf{g}_e^{(\odot)}} \frac{\partial\mathbf{g}_e^{(\odot)}}{\partial\boldsymbol{\sigma}_{i,e}} \frac{\partial\boldsymbol{\sigma}_{i,e}}{\partial\boldsymbol{\sigma}_e} \frac{\partial\boldsymbol{\sigma}_e}{\partial\tilde{\gamma}_e} + \sum_{e'=1}^{NE} \frac{\partial\langle\sigma_{PN}\rangle_k}{\partial\mathbf{g}_{e'}^{(\odot)}} \\ &\times \frac{\partial\mathbf{g}_{e'}^{(\odot)}}{\partial\boldsymbol{\sigma}_{i,e'}} \frac{\partial\boldsymbol{\sigma}_{i,e'}}{\partial\boldsymbol{\sigma}_{e'}} \frac{\partial\boldsymbol{\sigma}_{e'}}{\partial\mathbf{U}} \frac{d\mathbf{U}}{d\tilde{\gamma}_e} \end{aligned} \quad (44)$$

where, $\boldsymbol{\sigma}_{i,e} = [\sigma_1 \sigma_2 \sigma_3]$

The adjoint variable λ_k^T for the sensitivity analysis can be obtained from the derivatives of the static equilibrium equation as follows:

$$\mathbf{K} \frac{d\mathbf{U}}{d\tilde{\gamma}_e} = \frac{d\mathbf{f}}{d\tilde{\gamma}_e} - \frac{d\mathbf{K}}{d\tilde{\gamma}_e} \mathbf{U}, \quad \frac{d\mathbf{f}}{d\tilde{\gamma}_e} = 0 \quad (45)$$

$$\lambda_k^T = - \sum_{e'=1}^{NE} \frac{\partial\langle\sigma_{PN}\rangle_k}{\partial\mathbf{g}_{e'}^{(\odot)}} \frac{\partial\mathbf{g}_{e'}^{(\odot)}}{\partial\boldsymbol{\sigma}_{i,e'}} \frac{\partial\boldsymbol{\sigma}_{i,e'}}{\partial\boldsymbol{\sigma}_{e'}} \frac{\partial\boldsymbol{\sigma}_{e'}}{\partial\mathbf{U}} \mathbf{K}^{-1} \quad (46)$$

$$\mathbf{K}^T \lambda_k = - \sum_{e'=1}^{NE} \frac{\partial\langle\sigma_{PN}\rangle_k}{\partial\mathbf{g}_{e'}^{(\odot)}} \left(\frac{\partial\mathbf{g}_{e'}^{(\odot)}}{\partial\boldsymbol{\sigma}_{i,e'}} \frac{\partial\boldsymbol{\sigma}_{i,e'}}{\partial\boldsymbol{\sigma}_{e'}} \frac{\partial\boldsymbol{\sigma}_{e'}}{\partial\mathbf{U}} \right)^T \quad (47)$$

Note that we assume that the external force is independent of the design variables. Finally, by applying (47) to (44), the sensitivity of the p -norm of the failure criteria can be derived with the adjoint variable λ_k^T such that

$$\frac{d\langle\sigma_{PN}\rangle_k}{d\tilde{\gamma}_e} = \frac{\partial\langle\sigma_{PN}\rangle_k}{\partial\tilde{\gamma}_e} + \frac{\partial\langle\sigma_{PN}\rangle_k}{\partial\mathbf{g}_e^{(\odot)}} \frac{\partial\mathbf{g}_e^{(\odot)}}{\partial\boldsymbol{\sigma}_{i,e}} \frac{\partial\boldsymbol{\sigma}_{i,e}}{\partial\boldsymbol{\sigma}_e} \frac{\partial\boldsymbol{\sigma}_e}{\partial\tilde{\gamma}_e} + \lambda_k^T \frac{d\mathbf{K}}{d\tilde{\gamma}_e} \mathbf{U} \quad (48)$$

References

- [1] Allaire G, Jouve F, Maillot H. Topology optimization for minimum stress design with the homogenization method. *Struct Multidiscip Optim* 2004;28(2–3):87–98.
- [2] Hassani B, Hinton E. A review of homogenization and topology optimization I – homogenization theory for media with periodic structure. *Comput Struct* 1998;69(6):707–17.
- [3] Hassani B, Hinton E. A review of homogenization and topology optimization II – analytical and numerical solution of homogenization equations. *Comput Struct* 1998;69(6):719–38.
- [4] Hassani B, Hinton E. A review of homogenization and topology optimization III – topology optimization using optimality criteria. *Comput Struct* 1998;69(6):739–56.
- [5] Nishiwaki S, Frecker MI, Min SJ, Kikuchi N. Topology optimization of compliant mechanisms using the homogenization method. *Int J Numer Methods Eng* 1998;42(3):535–59.
- [6] Suzuki K, Kikuchi N. A homogenization method for shape and topology optimization. *Comput Methods Appl Mech Eng* 1991;93(3):291–318.
- [7] Bendsoe MP, Sigmund O. Material interpolation schemes in topology optimization. *Arch Appl Mech* 1999;69(9–10):635–54.
- [8] Bendsoe MP, Sigmund O. *Topology optimization: theory, methods, and applications*. Berlin, New York: Springer; 2003.
- [9] Sigmund O. A 99 line topology optimization code written in Matlab. *Struct Multidiscip Optim* 2001;21(2):120–7.
- [10] Amstutz S, Andra H. A new algorithm for topology optimization using a level-set method. *J Comput Phys* 2006;216(2):573–88.
- [11] Wang SY, Wang MY. Radial basis functions and level set method for structural topology optimization. *Int J Numer Methods Eng* 2006;65(12):2060–90.
- [12] Liu Z, Korvink JG, Huang R. Structure topology optimization: fully coupled level set method via FEMLAB. *Struct Multidiscip Optim* 2005;29(6):407–17.
- [13] Mei YL, Wang XM. A level set method for structural topology optimization and its applications. *Adv Eng Softw* 2004;35(7):415–41.
- [14] Wang X, Wang MY, Guo D. Structural shape and topology optimization in a level-set-based framework of region representation. *Struct Multidiscip Optim* 2004;27(1–2):1–19.
- [15] Wang MY, Wang XM, Guo DM. A level set method for structural topology optimization. *Comput Methods Appl Mech Eng* 2003;192(1–2):227–46.
- [16] van Dijk NP, Yoon GH, van Keulen F, Langelaar M. A level-set based topology optimization using the element connectivity parameterization method. *Struct Multidiscip Optim* 2010;42(2):269–82.
- [17] Yoon GH. Maximizing the fundamental eigenfrequency of geometrically nonlinear structures by topology optimization based on element connectivity parameterization. *Comput Struct* 2010;88(1–2):120–33.
- [18] Yoon GH, Kim YY. Topology optimization of material-nonlinear continuum structures by the element connectivity parameterization. *Int J Numer Methods Eng* 2007;69(10):2196–218.

- [19] Yoon GH, Joungh YS, Kim YY. Optimal layout design of three-dimensional geometrically non-linear structures using the element connectivity parameterization method. *Int J Numer Methods Eng* 2007;69(6):1278–304.
- [20] Yoon GH, Kim YY. The element connectivity parameterization formulation for the topology design optimization of multiphysics systems. *Int J Numer Methods Eng* 2005;64(12):1649–77.
- [21] Yoon GH, Kim YY. Element connectivity parameterization for topology optimization of geometrically nonlinear structures. *Int J Solids Struct* 2005;42(7):1983–2009.
- [22] Bruggi M. On an alternative approach to stress constraints relaxation in topology optimization. *Struct Multidiscipl Optim* 2008;36(2):125–41.
- [23] Bruggi M, Venini P. A mixed FEM approach to stress-constrained topology optimization. *Int J Numer Methods Eng* 2008;73(12):1693–714.
- [24] Cheng G, Jiang Z. Study on topology optimization with stress constraints. *Eng Optim* 1992;20(2):129–48.
- [25] Cheng GD, Guo X. Epsilon-relaxed approach in structural topology optimization. *Struct Optim* 1997;13(4):258–66.
- [26] Duysinx P, Bendsoe MP. Topology optimization of continuum structures with local stress constraints. *Int J Numer Methods Eng* 1998;43(8):1453–78.
- [27] Le C, Norato J, Bruns T, Ha C, Tortorelli D. Stress-based topology optimization for continua. *Struct Multidiscipl Optim* 2010;41(4):605–20.
- [28] Paris J, Navarrina F, Colominas I, Casteleiro M. Topology optimization of continuum structures with local and global stress constraints. *Struct Multidiscipl Optim* 2009;39(4):419–37.
- [29] Paris J, Navarrina F, Colominas I, Casteleiro M. Block aggregation of stress constraints in topology optimization of structures. *Adv Eng Softw* 2010;41(3):433–41.
- [30] Svanberg K, Werme M. Sequential integer programming methods for stress constrained topology optimization. *Struct Multidiscipl Optim* 2007;34(4):277–99.
- [31] Yang RJ, Chen CJ. Stress-based topology optimization. *Struct Optim* 1996;12(2–3):98–105.
- [32] Rozvany GIN, Sobieszcanskisobieski J. New optimality criteria methods – forcing uniqueness of the adjoint strains by corner-rounding at constraint intersections. *Struct Optim* 1992;4(3–4):244–6.
- [33] Querin OM, Victoria M, Marti P. Topology optimization of truss-like continua with different material properties in tension and compression. *Struct Multidiscipl Optim* 2010;42(1):25–32.
- [34] Duysinx P. Topology optimization with different stress limits in tension and compression, In: *Proceedings of the third world congress of structural and multidisciplinary optimization (WCSMO3)*, Buffalo, NY, USA, 1999.
- [35] Rozvany GIN. Some shortcomings in Michell's truss theory – reply. *Struct Optim* 1997;13(2–3):203–4.
- [36] Luo YJ, Kang Z. Topology optimization of continuum structures with Drucker–Prager yield stress constraints. *Comput Struct* 2012;90–91:65–75.
- [37] Bruggi M, Duysinx P. Topology optimization for minimum weight with compliance and stress constraints. *Struct Multidiscipl Optim* 2012. <http://dx.doi.org/10.1007/s00158-012-0759-7>.
- [38] Qiu CY, Li XS. A note on the derivation of global stress constraints. *Struct Multidiscipl Optim* 2010;40(1–6):625–8.
- [39] Verbart A, Dijk N, Tin LD, Langelaar M, Keulen F. Effect of design parameterization and relaxation on model responses in topology optimization with stress constraints, In: *Proceedings of 9th world congress on structural and multidisciplinary optimization*, Shizuoka, Japan, 2011.
- [40] Rossow MP, Taylor JE. A finite element method for the optimal design of variable thickness sheets. *AIAA* 1973;11(11):1566–7.
- [41] Budynas RG, Nisbett JK. Shigley's mechanical engineering design. 9th ed. New York: McGraw-Hill; 2011.
- [42] Jeong SH, Choi DH, Yoon GH. Separable stress interpolation scheme for stress-based topology optimization with multiple materials, in review, 2011.
- [43] Svanberg K. The method of moving asymptotes – a new method for structural optimization. *Int J Numer Methods Eng* 1987;24(2):359–73.